The Influence of Local Feedbacks and Northward Heat Transport on the Equilibrium Arctic Climate Response to Increased Greenhouse Gas Forcing

JENNIFER E. KAY AND MARIKA M. HOLLAND

National Center for Atmospheric Research, Boulder, Colorado

CECILIA M. BITZ AND EDWARD BLANCHARD-WRIGGLESWORTH

Department of Atmospheric Sciences, University of Washington, Seattle, Washington

ANDREW GETTELMAN, ANDREW CONLEY, AND DAVID BAILEY

National Center for Atmospheric Research, Boulder, Colorado

(Manuscript received 19 October 2011, in final form 10 February 2012)

ABSTRACT

This study uses coupled climate model experiments to identify the influence of atmospheric physics [Community Atmosphere Model, versions 4 and 5 (CAM4; CAM5)] and ocean model complexity (slab ocean, full-depth ocean) on the equilibrium Arctic climate response to an instantaneous CO_2 doubling. In slab ocean model (SOM) experiments using CAM4 and CAM5, local radiative feedbacks, not atmospheric heat flux convergence, are the dominant control on the Arctic surface response to increased greenhouse gas forcing. Equilibrium Arctic surface air temperature warming and amplification are greater in the CAM5 SOM experiment than in the equivalent CAM4 SOM experiment. Larger $2 \times CO_2$ radiative forcing, more positive Arctic surface albedo feedbacks, and less negative Arctic shortwave cloud feedbacks all contribute to greater Arctic surface warming and sea ice loss in CAM5 as compared to CAM4. When CAM4 is coupled to an active full-depth ocean model, Arctic Ocean horizontal heat flux convergence increases in response to the instantaneous CO_2 doubling. Though this increased ocean northward heat transport slightly enhances Arctic sea ice extent loss, the representation of atmospheric processes (CAM4 versus CAM5) has a larger influence on the equilibrium Arctic surface climate response than the degree of ocean coupling (slab ocean versus full-depth ocean). These findings underscore that local feedbacks can be more important than northward heat transport for explaining the equilibrium Arctic surface climate response and response differences in coupled climate models. That said, the processes explaining the equilibrium climate response differences here may be different than the processes explaining intermodel spread in transient climate projections.

1. Motivation and research questions

Arctic amplification, broadly defined as greater-than-global Arctic warming in response to external forcing and/or internal climate variability, is ubiquitous in climate models and observations (Manabe and Stouffer 1980; Miller et al. 2010; Serreze and Barry 2011). Despite a long and rich history of numerical model experiments and observational analysis, the relative importance of processes controlling Arctic amplification is still subject to debate. Because the definition of Arctic amplification affects the identification of processes explaining Arctic amplification, we begin by defining Arctic amplification for the purposes of this study as the greater-than-global Arctic air or surface temperature warming in response to increased greenhouse gases.

Both local feedbacks, such as the canonical positive surface albedo feedback (SAF), and heat flux convergence have been shown to affect Arctic warming and amplification in response to increased greenhouse gases. In fact, shortwave feedbacks (e.g., Hall 2004, hereafter H04; Winton 2006, hereafter W06; Gorodetskaya et al. 2008, hereafter G08), longwave feedbacks (e.g., Boé et al. 2009, hereafter B09) and heat flux convergence (e.g., Alexeev et al. 2005; Graversen and Wang 2009; Holland and Bitz 2003, hereafter HB03; Ridley et al. 2007,

Corresponding author address: Jennifer E. Kay, NCAR Climate and Global Dynamics Division, P.O. Box 3000, Boulder, CO 80307. E-mail: jenkay@ucar.edu

DOI: 10.1175/JCLI-D-11-00622.1

TABLE 1. Model description and temperature response to a CO_2 doubling.

Model	Description	Resolution	Climate sensitivity (K)*	Global surface warming (K)	Arctic surface warming (K)	Arctic 700-hPa warming (K)
CAM5	CAM5 slab ocean model	1.9x2.5_gx1v6	4.0	4.0	10.2	5.1
CAM4	CAM4 slab ocean model	1.9x2.5_gx1v6	3.1	3.1	7.0	4.2
$CAM4_{hi}$	CAM4 slab ocean model	0.9x1.25_gx1v6	3.2	3.1	6.6	3.8
CCSM4	CAM4 full-depth ocean model	0.9x1.25_gx1v6	2.9	2.5	6.5	2.9

* The climate sensitivity is the equilibrium global surface temperature response to a CO_2 doubling. The CCSM4 climate sensitivity was estimated using a regression between the globally averaged TOA radiation imbalance and surface temperature (Gregory et al. 2004), a method with known deficiencies (Winton et al. 2010). The CAM4 and CAM5 climate sensitivities are estimated from the average surface temperature increase during the last 10 years of the slab ocean model runs. The $CAM4_{hi}$ climate sensitivity is from Bitz et al. (2012b).

hereafter R07; Mahlstein and Knutti 2011) have all been identified as key processes. Given this lack of consensus, there is a continued need to rank and understand the importance of processes controlling Arctic greenhouse warming and amplification in coupled climate models.

Many techniques have been used to identify the processes controlling modeled Arctic greenhouse warming and amplification. Some studies have focused on multimodel correlation analysis (e.g., HB03), others have used feedback parameter analysis (e.g., W06), while still others have used sensitivity tests to isolate the relative importance of individual processes (e.g., H04). Previous studies have confirmed that SAF is important, but that it is not the only process-explaining modeled Arctic greenhouse response. For example, H04 used suppressed SAF experiments to show that SAF is responsible for half of the equilibrium Arctic surface warming response to a CO_2 doubling in one model.

Unfortunately, it is difficult to cleanly isolate processes controlling Arctic greenhouse warming and amplification in coupled model experiments. This is especially true in model sensitivity studies that eliminate or change the relative importance of an individual process to identify its importance. Simply put, local processes affect temperature gradients, and thus local feedbacks and atmospheric horizontal heat convergence are coupled (e.g., Hwang et al. 2011). One striking implication of this coupling is that suppressing individual feedbacks leads to changes in northward heat transport, which may in turn affect the strength of local feedbacks. For example, suppressed SAF experiments may overemphasize the importance of atmospheric heat flux convergence increases driven by atmospheric latent energy increases because they underestimate compensating dry static energy decreases resulting from positive SAF feedbacks.

Motivated and informed by the above discussion, we focus on understanding the Arctic, herein defined as 70°–90°N following Serreze et al. (2007), equilibrium response to an instantaneous CO_2 doubling in coupled climate model experiments with different atmospheric components and different degrees of ocean coupling. Informed by a comprehensive set of northward heat transport and feedback parameter diagnostics, two central questions are addressed. First, which processes explain the *equilibrium Arctic response* to $2 \times CO_2$ in the *coupled* model experiments? We find that local feedbacks, not heat transport changes, are the dominant control on the modeled equilibrium Arctic surface warming and amplification. Second, which processes explain the *equilibrium Arctic response* to $2 \times CO_2$ *differences* between the *coupled* model experiments? We find that the atmospheric model physics is more important than the complexity of the ocean model (slab ocean model versus full-depth ocean model) for explaining Arctic surface warming and amplification differences. In particular, the $2 \times CO_2$ forcing and the influence of Arctic clouds on shortwave feedbacks explain the largest identified greenhouse warming differences.

2. Coupled climate model experiments

a. Description of climate model experiments

This study uses a unique set of coupled climate model experiments to isolate the influence of atmospheric physics and ocean model complexity on the equilibrium Arctic climate response to $2 \times CO_2$ (Table 1). All experiments used the same Community Climate System Model, version 4 (CCSM4) (Gent et al. 2011) land, ocean, and sea ice components with one of two versions of the Community Atmosphere Model (CAM) released with Community Earth System Model (CESM) version 1: CAM4 (Neale et al. 2011a) or CAM5 (Neale et al. 2011b). Although CAM4 and CAM5 were both released in 2010, their only shared physical parameterization is the deep convection scheme (see Kay et al. 2012, Table 1). The atmospheric dynamical core in CAM4 and CAM5 is identical, allowing a clear identification of the influence of the CAM4 and CAM5 physical parameterizations on our results. The nonatmospheric CCSM4 model components were also identical, the only exception being that the CAM5 experiments did not have prognostic

carbon–nitrogen cycling in the land model component. All model components had optimized parameter settings to simulate present-day climate and transient twentieth-century climate change.

Three slab ocean model (SOM) experiments (CAM5, CAM4, and $CAM4_{hi}$) and one active full-depth ocean model experiment (CCSM4) were run. All experiments used a prognostic sea ice model, mixed layer heat storage, and atmosphere–surface ocean coupling, and therefore captured many important coupled Arctic processes. All model experiments also included ocean heat transport. The prescribed ocean heat fluxes in the SOM experiments, often called Q-FLUXES, were derived from the ocean heat divergence in a stable and well-equilibrated preindustrial climate model integration with an active full-depth ocean and the equivalent atmospheric model. Because the Q-FLUXES were fixed, ocean heat transport in the SOM integrations could not respond to forcing changes. The SOM formulation used here matches Bitz et al. (2012b) and differs from an earlier SOM formulation (Kiehl et al. 2006). A full-depth ocean experiment with CAM5 was not available, but experiments using CAM4 were analyzed to assess the influence of ocean heat transport changes.

For each model experiment, a control integration with constant 1850 forcing was completed. All control integrations had balanced and stable top of atmosphere (TOA) radiative fluxes. For each control integration, we then ran a sensitivity experiment by instantaneously doubling the CO_2 concentration from the 1850 value of 284.7 to 569.4 ppmv. Because the TOA radiative forcing resulting from a CO_2 doubling (Q_{2xCO2}, W m^{-2}) depends both on the radiative transfer code and on the climate state, we estimated the Q_{2xCO2} separately for CAM4 and CAM5 using one year of offline radiative transfer calculations. We allowed temperatures above the tropopause (definition from Reichler et al. 2003) to adjust using an assumption of fixed dynamical heating (Hansen et al. 2005). We found that the CAM4 global Q_{2xCO2} (3.5 W m^{-2}) was smaller than the CAM5 global Q_{2xCO2} (3.8 W m^{-2}), but that both global CAM Q_{2xCO2} values were within 10% of 3.7 W m^{-2}, the established uncertainty in climate model global Q_{2xCO2} (Solomon et al. 2007).

After 50 years, the SOM integrations had fully equilibrated to the $2 \times CO_2$ forcing. Quick equilibration was expected because the SOM integrations had no mechanism for ocean heat uptake beneath the ocean mixed layer. After 300 years, a residual TOA imbalance of $\sim$0.5 W m^{-2} remained in the $2 \times CO_2$ CCSM4 integration, an indication that the simulation was not in equilibrium. For all model experiments, the $2 \times CO_2$ response was quantified by averaging the last 10 years of the model integrations (years 51–60 for the SOM integrations, years 291–300 for CCSM4). For the CCSM4, averages over the last 10 years and the last 50 years were also compared to assess response robustness.

b. *Equilibrium climate response to a carbon dioxide doubling*

We begin by documenting the equilibrium temperature response to $2 \times CO_2$ as a function of latitude and height above the surface in all experiments. Both air temperature warming and amplification, that is, the local (north of X°N) warming normalized by the global warming, are shown.

CAM5 has the greatest surface warming of the coupled models examined in this study (Fig. 1a). At 700 hPa the same ranking as the surface warming is evident; namely, CAM5 has the most warming and CCSM4 has the least warming, but in each model version the warming at 700 hPa is smaller than at the surface (Table 1, Fig. 1b). The relationship between the Arctic and global warming magnitude in these models is consistent with previous studies (e.g., Gregory et al. 2002): models with more global warming have more Arctic warming (Table 1).

Comparing two SOM experiments with identical physics but different horizontal resolutions, CAM4 and $CAM4_{hi}$, demonstrates that resolution has a small impact on the warming response to $2 \times CO_2$ (Fig. 1, Table 1) In contrast, coupling to the deep ocean affects the realized $2 \times CO_2$ warming. By years 291–300 the global (Arctic) surface temperature in CCSM4 increases by 2.5 K (6.5 K), which is 0.6 K (0.1 K) less than the equilibrium warming in $CAM4_{hi}$. At northern latitudes CCSM4 exhibits less warming from 30° to 75°N than CAM4 or $CAM4_{hi}$ (Fig. 1a). This relatively weak warming in CCSM4 reflects the multicentury time scale required to reach equilibrium with an active full-depth ocean (e.g., Solomon et al. 2009). That the Arctic surface warming in CCSM4 is only 0.1 K less than the equilibrium surface warming in $CAM4_{hi}$ suggests that CCSM4 would have a larger equilibrium Arctic warming than its SOM equivalent. Assuming an equivalent Q_{2xCO2} for CCSM4 and CAM4 (3.5 W m^{-2}), and that the ratio of Arctic surface warming per unit global TOA forcing [6.5 K/(3.0 W m^{-2}) = 2.2 K (W m^{-2})$^{-1}$] remains constant for the residual global TOA imbalance (0.5 W m^{-2}), an additional degree of Arctic surface warming should occur when CCSM4 reaches equilibrium. Taking this unrealized CCSM4 surface warming into account, the equilibrium Arctic surface warming in CCSM4 would still be 2.7 K smaller than in CAM5.

As expected, Arctic amplification in response to $2 \times CO_2$ is present in all of the model experiments. Amplification is evident poleward of approximately 50°N;

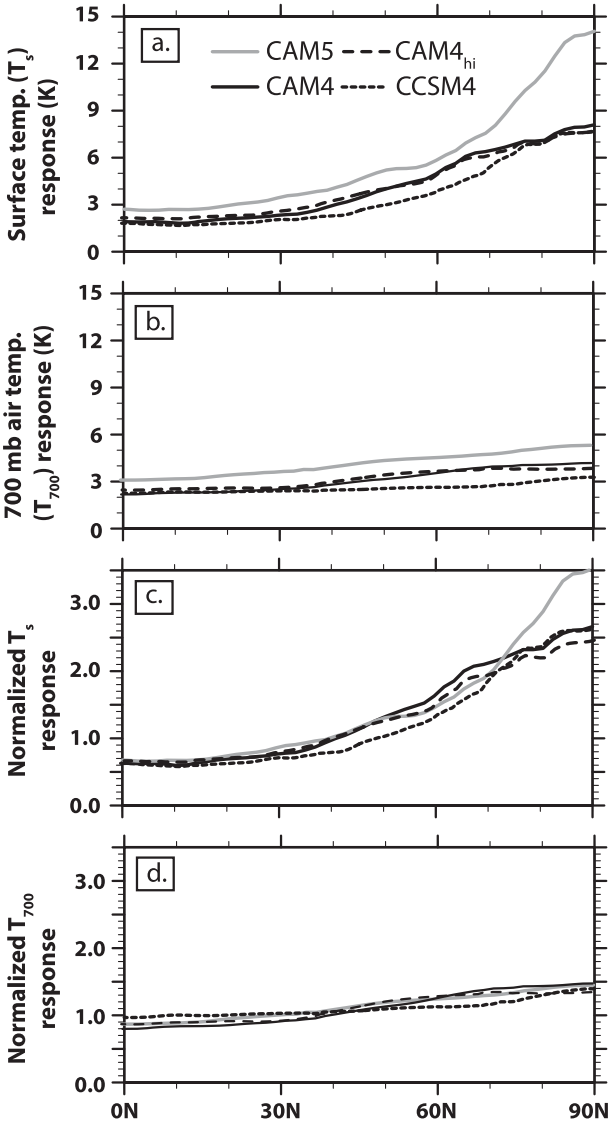

FIG. 1. Northern Hemisphere zonal annual mean equilibrium warming response to $2 \times CO_2$: (a) surface temperature, (b) 700-mb air temperature, (c) surface temperature amplification (local response normalized by global response), and (d) 700-mb air temperature amplification.

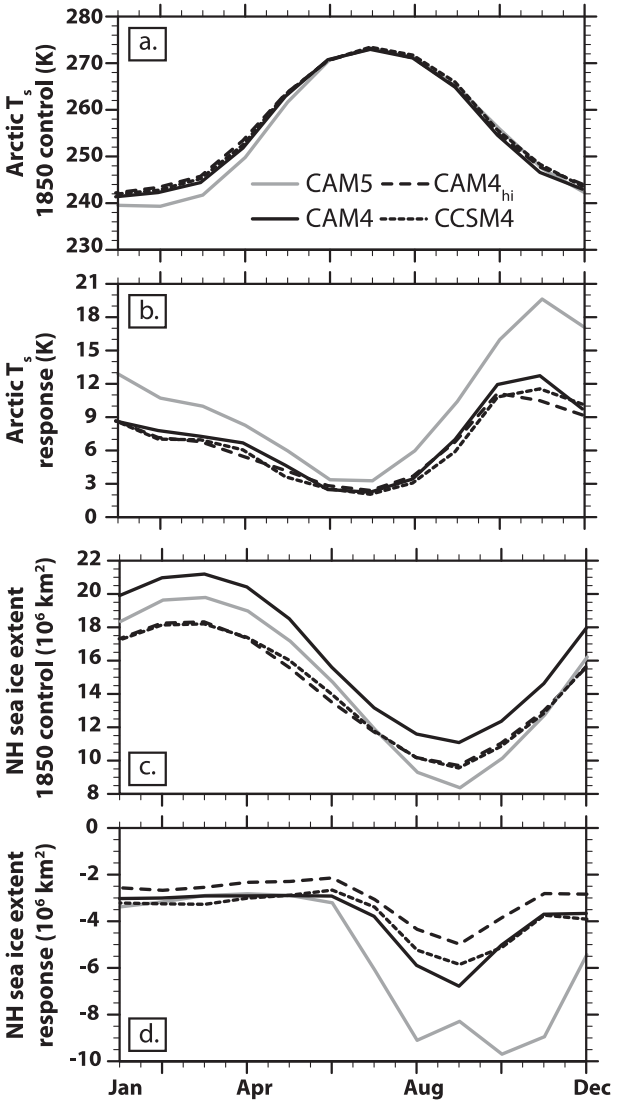

FIG. 2. Monthly equilibrium Arctic 1850 climate and response to $2 \times CO_2$ in all coupled climate models (Table 1): (a),(b) surface temperature and warming and (c),(d) Northern Hemisphere (NH) sea ice extent and extent loss.

however, amplification is significantly less pronounced at 700 mb than at the surface (Figs. 1c,d). Poleward of 70°N, CAM5 has more surface amplification than any of the coupled models using the CAM4 physical parameterizations, but 700-hPa amplification is similar in all of the coupled models. The spread in the maximum Arctic surface temperature amplification (2.5–3.5) is not large when compared to the range reported in HB03 for fully coupled transient climate model simulations (1.5–4.5). All models examined here exhibit maximum warming over the Arctic basin, consistent with the high Arctic amplification models in HB03. Comparison of CAM4$_{hi}$ and CCSM4 shows that coupling with the deep ocean slightly enhances Arctic surface temperature amplification: a result consistent with HB03 and CCSM3 (Bitz et al. 2006).

Because seasonality of the Arctic $2 \times CO_2$ response is known to be important (Manabe and Stouffer 1980), Fig. 2 shows the monthly Arctic surface temperatures, warming, sea ice extent, and sea ice extent loss in all model experiments. Though all models exhibit similar response seasonality, CAM5 has more late summer sea ice loss and more fall and early winter surface warming than any model with CAM4 (Figs. 2b,d). At $2 \times CO_2$, CAM5 is seasonally ice free, having no Arctic sea ice from August

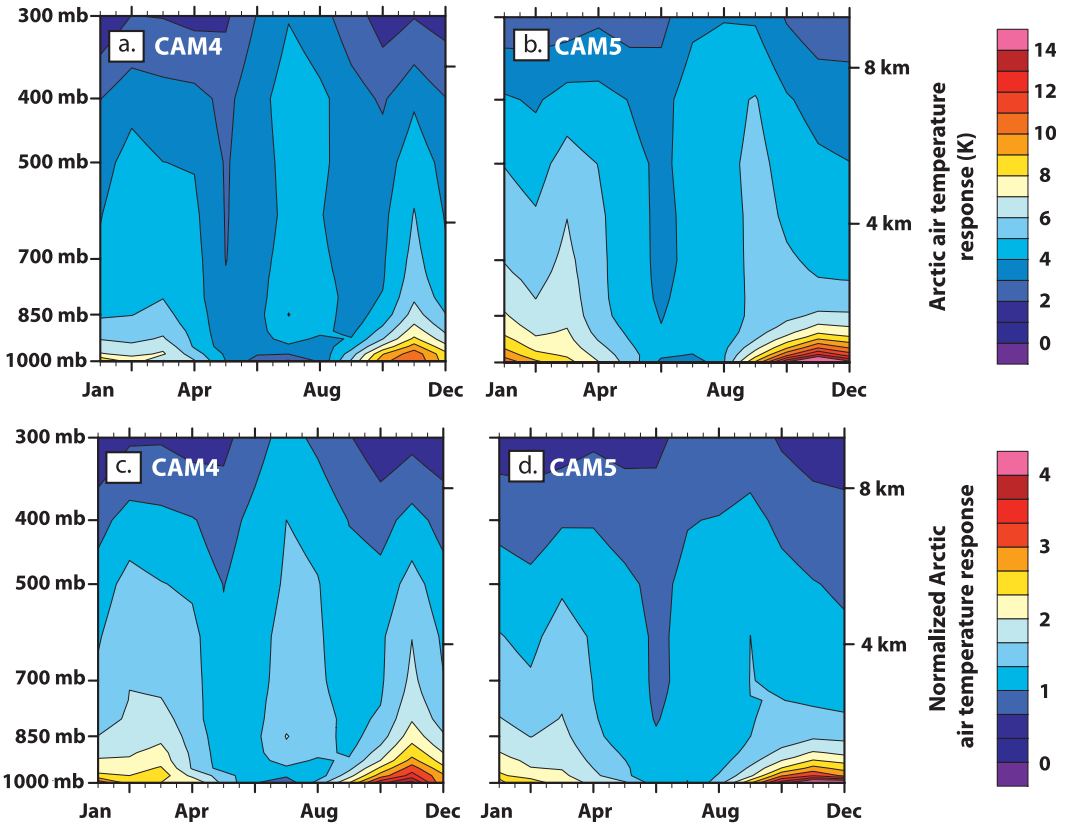

FIG. 3. Vertical monthly mean Arctic (70°–90°N) equilibrium warming response to 2 × CO_2 in the slab ocean models: (a) CAM4 air temperature, (d) CAM5 air temperature, (c) CAM4 air temperature amplification (local response normalized by global response), and (d) CAM5 air temperature amplification.

through October, and also loses winter sea ice along the margins of the Arctic Ocean basin (not shown). In contrast, at 2 × CO_2, CAM4 retains perennial ice cover and the winter sea ice extent loss is mainly confined to outside the Arctic Ocean basin (not shown). In summary, the atmospheric model physics (CAM4 versus CAM5) has a greater influence on Arctic warming than coupling to an active deep ocean (CCSM4 versus $CAM4_{hi}$). By comparing $CAM4_{hi}$ and CCSM4, we do, however, find evidence that an active deep ocean enhances Arctic sea ice extent loss in all months, producing up to a modest 1.3 million square kilometer difference in the monthly ice extent loss.

We have shown the largest climate response differences result from the representation of atmospheric processes (CAM4 versus CAM5), not resolution (CAM4 versus $CAM4_{hi}$) or coupling to the deep ocean ($CAM4_{hi}$ versus CCSM4). Thus, we next further contrast the monthly Arctic temperature response in CAM4 and CAM5 as a function of height above the surface (Fig. 3, Fig. 4) and surface type (Fig. 5). We find important seasonal, geographic, and vertical variations in the 2 × CO_2 warming magnitude but, interestingly, we find that CAM5 has more Arctic warming than CAM4 during all seasons, throughout the troposphere, and over most surface types.

Fig. 3 shows that both CAM4 and CAM5 exhibit the classical signature of surface-based Arctic greenhouse warming and amplification (Manabe and Stouffer 1980; Serreze et al. 2009), namely, cold season surface warming that exceeds warming aloft and is largest in the late fall and early winter. In contrast, warming aloft exceeds surface warming during midsummer. In both models, Arctic warming patterns match Arctic amplification patterns from the surface to 300 mb.

Because B09 attribute intermodel spread in Arctic anthropogenic greenhouse response to longwave feedbacks differences that are tied to the stability of the lower atmosphere, Fig. 4 shows the monthly evolution of Arctic stability and stability response in both models. Comparing Figs. 3 and 4 shows that fall and winter near-surface stability declines are tightly coupled to surface warming, while summer near-surface stability increases result from air temperature increases above the surface.

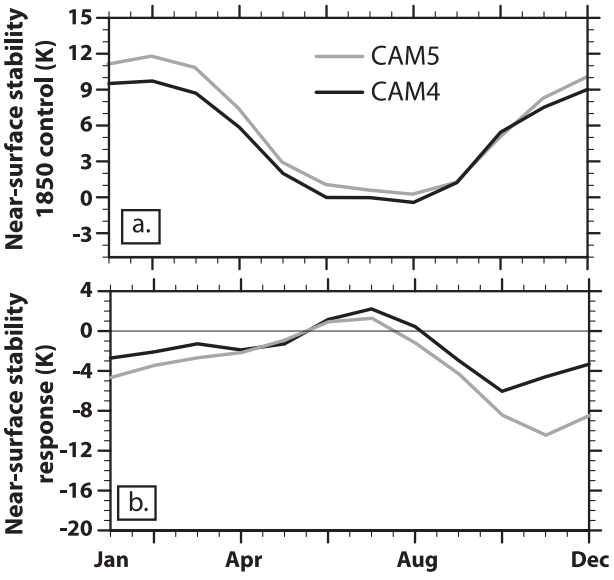

FIG. 4. Monthly Arctic near-surface stability (temperature at 925 hPa minus surface temperature): (a) 1850 control and (b) response to 2 × CO_2.

Contrary to what was found in B09, CAM5 has greater warming than CAM4, but a higher control climate winter near-surface stability, especially over ice-free areas, an important geographic factor to consider, as discussed by Medeiros et al. 2011.

In our experiments, the greatest Arctic 2 × CO_2 warming and warming differences occur at the surface. Surface type has a substantial influence on the magnitude and seasonality of the surface warming, as seen in Fig. 5. Not surprisingly, the largest surface warming and the largest warming differences between CAM4 and CAM5 occur during late summer to early winter in transition regimes, that is, regions that became newly ice free. Indeed, transition regimes are key for explaining why CAM5 has more Arctic 2 × CO_2 warming than CAM4. Not only does CAM5 have 10 K greater late fall warming in transition regimes than CAM4, transition regimes also occur more frequently in CAM5 than in CAM4. In contrast, midsummer warming is relatively modest in transition regimes. Summer is the season in which the Arctic land warms more than any other regime, but differences between CAM4 and CAM5 warming over land during summer (and also spring) are relatively small. Persistent ice-covered regimes exhibit warming that is similar to the Arctic average. The least warming and least seasonality in the Arctic warming response occurs in persistent open-water regimes, that is, in the North Atlantic; however, these persistent open-water regimes warm more in CAM5 than in CAM4 in every season except for summer.

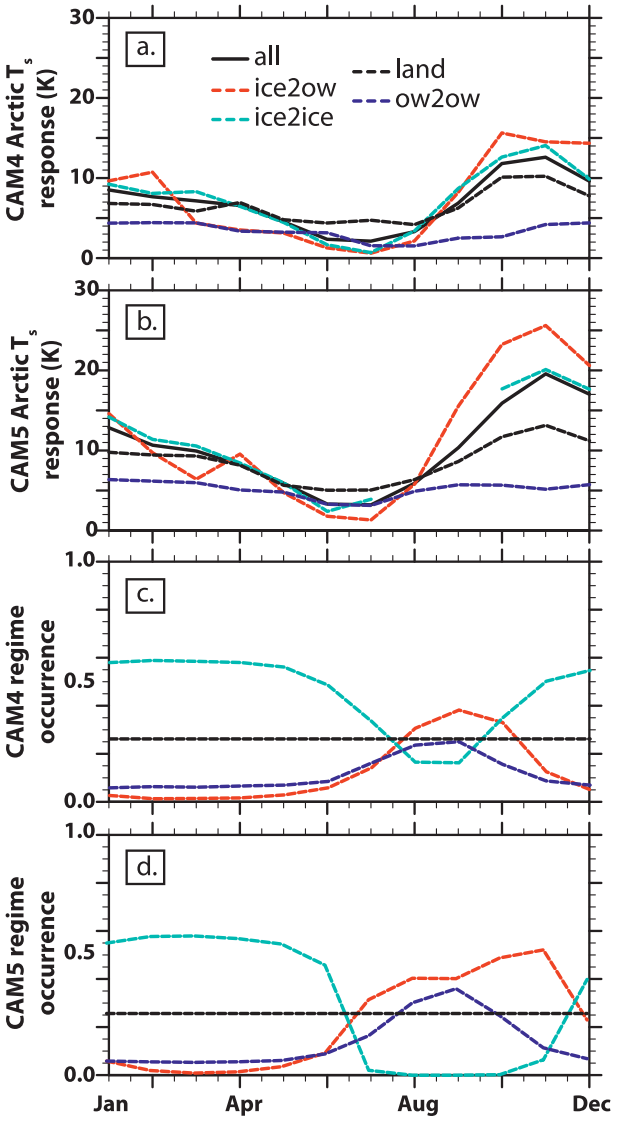

FIG. 5. Monthly mean Arctic regimes and surface warming response to 2 × CO_2: (a) CAM4 surface warming by regime, (b) CAM5 surface warming by regime, (c) CAM4 regime occurrence, and (d) CAM5 regime occurrence. Regimes are defined for each month as follows. Transition regions ("ice2ow") are ice-covered at 1 × CO_2 but open water at 2 × CO_2. Ice-covered regions ("ice2ice") are ice-covered at both 1 × CO_2 and 2 × CO_2. Open water regions ("ow2ow") are open water at both 1 × CO_2 and 2 × CO_2. Land regions ("land") are land at both 1 × CO_2 and 2 × CO_2. Model grid cells are ice-covered if the sea ice fraction equals or exceeds 0.15, open water if the sea ice fraction is less than 0.15, and land if the land fraction exceeds 0.50.

3. Explaining the climate response and response differences

Having introduced the climate model experiments and documented their Arctic climate response to an instantaneous CO_2 doubling (Table 1, Figs. 1–5), we next

develop and apply targeted diagnostics to understand the responses. Because the largest 2 × CO_2 response and response differences are found at the surface (Fig. 3), we focus on identifying the *dominant* processes controlling Arctic *surface warming* and *amplification* in the model experiments. We begin by presenting changes in Arctic heat flux convergence in CAM4, CAM5, and CCSM4 (section 3a). Then we complete a feedback parameter analysis to identify the relative importance of individual feedback processes in CAM4 and CAM5 (section 3b). Finally, we examine the energy budgets, clouds, and sea ice in the 1850 controls of CAM4 and CAM5 to identify aspects of their mean states that are consistent with their 2 × CO_2 response differences (section 3c).

a. *The influence of northward heat transport on the equilibrium climate response*

1) METHODS

Northward heat transport (NHT, watts) into the Arctic basin results from atmospheric northward heat transport (NHT_{atm}), oceanic northward heat transport (NHT_{ocn}), and the latent heat associated with sea ice export (NHT_{ice}). NHT_{atm} can be separated into latent heat transport ($NHT_{atm\text{-}latent}$) and dry static energy heat transport ($NHT_{atm\text{-}dse}$). In this study, NHT_{ice} and NHT_{ocn} were calculated at each time step within the CESM code; however, atmospheric model grid interpolation and the sequencing of calculations limited the accuracy of in-line NHT_{atm} calculations. Thus, the appendix details the methods used to calculate total and atmospheric heat flux convergence for equilibrium and transient conditions using energy budgets and residual methods. For example, we calculated vertically and zonally integrated heat flux convergence based on the fact that, in steady state, horizontal heat flux convergence across a latitude band is balanced by the net TOA flux poleward of that latitude:

$$\mathrm{NHT} = -2\pi R_e^2 \int_{\varphi}^{\pi/2} N \cos(\varphi)\, d\varphi, \qquad (1)$$

where R_e is the radius of the earth (m), N is the TOA net energy flux (W m^{-2}), and φ is the latitude (radians).

2) SLAB OCEAN EXPERIMENTS RESULTS

We first examine the equilibrium NHT changes in the models with largest modeled Arctic 2 × CO_2 warming and amplification response differences, namely, CAM4 and CAM5. We find that neither equilibrium (Fig. 6) nor transient (Fig. 7) NHT changes can explain the greater Arctic 2 × CO_2 warming and amplification in CAM5 as compared to CAM4.

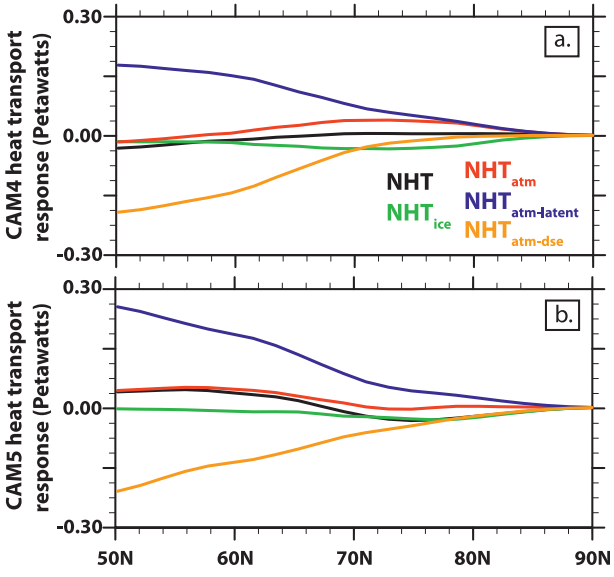

FIG. 6. Zonal mean northward heat transport: (a) CAM4 equilibrium NHT response to 2 × CO_2, and (b) as in (a), but for CAM5.

In both models the equilibrium NHT 2 × CO_2 response at 70°N (Fig. 6) is small when compared to the control climate NHT (not shown). By construct, the change in NHT_{ocn} in the SOMs is zero. As expected, NHT_{ice} at 70°N decreases in the warmer climates because sea ice export out of the Arctic basin is reduced (Serreze et al. 2007). NHT_{atm} changes at 70°N are small because $NHT_{atm\text{-}latent}$ increases are compensated by $NHT_{atm\text{-}dse}$ decreases, a typical occurrence in climate models (Bitz et al. 2012a; Hwang et al. 2011). Of particular importance, NHT_{atm} changes at 70°N do not explain the greater equilibrium 2 × CO_2 response in CAM5: CAM4 has a small increase in NHT_{atm} while CAM5 has similar NHT_{atm} in the control and 2 × CO_2 climates. Interestingly, NHT_{atm} changes at 70°N do not act in concert with changes at lower latitudes. South of the Arctic basin (~50°–65°N), CAM5 has larger $NHT_{atm\text{-}latent}$ increases than CAM4, and thus CAM5 has larger NHT_{atm} increases than CAM4.

Because transient NHT_{atm} responses can differ from equilibrium NHT_{atm} responses (e.g., idealized SOM experiments in Alexeev et al. 2005 and Langen and Alexeev 2007), we next examine the transient response to 2xCO_2 in CAM4 and CAM5 (Fig. 7). The majority of the surface warming occurs in the first 20 years of the model integrations (Fig. 7a). During this transient period, CAM5 has more surface warming and larger increases in the net TOA flux than CAM4 (Figs. 7a,b). During both transient and equilibrium periods, CAM4 has small increases in NHT_{atm} while the NHT_{atm} in CAM5 remains nearly constant (Figs. 7c,d).

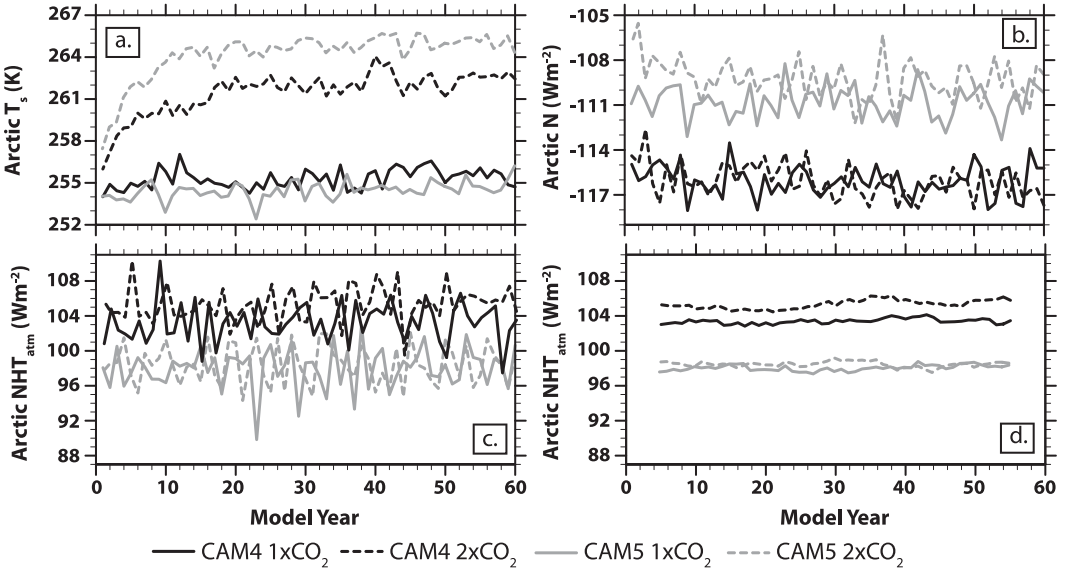

FIG. 7. Transient Arctic evolution in the CAM4 and CAM5 integrations: (a) surface temperature, (b) top-of-atmosphere net energy flux, (c) atmospheric northward heat transport at 70°N, and (d) as in (c) but with a 10-yr running mean applied to the time series.

3) COUPLING TO AN ACTIVE FULL-DEPTH OCEAN

We next address if coupling to a full-depth ocean model changes the heat transport response to 2 × CO_2 (Fig. 8). Surprisingly, we find that the total NHT response from 50° to 90°N is similar (within 0.02 petawatts) in slab and full-depth ocean models with equivalent atmospheric processes and resolution, namely, $CAM4_{hi}$ and CCSM4 (Fig. 8a). To further understand this similar NHT response and its implications for climate response differences (Figs. 1 and 2), we break down NHT into contributions from the ocean, sea ice, and atmosphere (Figs. 8b,c).

Like CCSM3 (Bitz et al. 2006), NHT_{ocn} in CCSM4 increases in response to increased CO_2 forcing, which may explain the increased sea ice loss in CCSM4 as compared to its slab equivalent $CAM4_{hi}$ (Fig. 2). The CCSM4 NHT_{ocn} increases are largely compensated by NHT_{ice} decreases, resulting in a small change in nonatmospheric NHT ($NHT_{non\text{-}atm}$) poleward of 60°N (Fig. 8b). Because NHT_{ocn} is fixed in the slab ocean model integrations, NHT_{ice} decreases resulting from reduced ice export in a warmer climate are the only process influencing $NHT_{non\text{-}atm}$ in $CAM4_{hi}$.

Given that the total NHT response is nearly identical in the $CAM4_{hi}$ and CCSM4 experiments, the differing $NHT_{non\text{-}atm}$ response in the slab and full-depth ocean models must be compensated by a differing NHT_{atm} response. Indeed, NHT_{atm} at 70°N in $CAM4_{hi}$ increases while NHT_{atm} at 70°N in CCSM4 decreases (Fig. 8c). Poleward of 70°N this NHT_{atm} response difference is due to larger $NHT_{atm\text{-}latent}$ increases in $CAM4_{hi}$ than in CCSM4. In summary, compensating changes in the atmospheric and ocean heat flux convergence produce a near-equivalent total NHT response at 70°N in $CAM4_{hi}$ and CCSM4 and may help explain the similar Arctic climate response in the two models (Fig. 1, Fig. 2). Even though CCSM4 has not reached equilibrium, Arctic NHT is similar during last 50 years and the last 10 years of the integration, suggesting that the NHT in CCSM4 after 300 years and at equilibrium would be similar.

b. Feedback analysis

Having established that NHT differences do not explain the largest Arctic climate response differences in this study, we next present feedback parameter analyses to identify the processes that do control the Arctic surface climate response in CAM4 and CAM5. The magnitude of a feedback parameter can be thought of as the efficiency of fluxing heat out the TOA for a given temperature change. It is assumed that processes that affect TOA energy fluxes the most are, in turn, the most important for explaining the model response to 2 × CO_2. We start with global feedback parameter analysis in section 3b(1). We then present a simple extension of the global framework for the Arctic in 3b(2). Throughout the text, results are compared to Gettelman et al. 2012, who analyze global feedback parameters in CAM4 and CAM5 using the radiative kernel technique (Soden and Held 2006) with radiative kernels derived from CAM3.

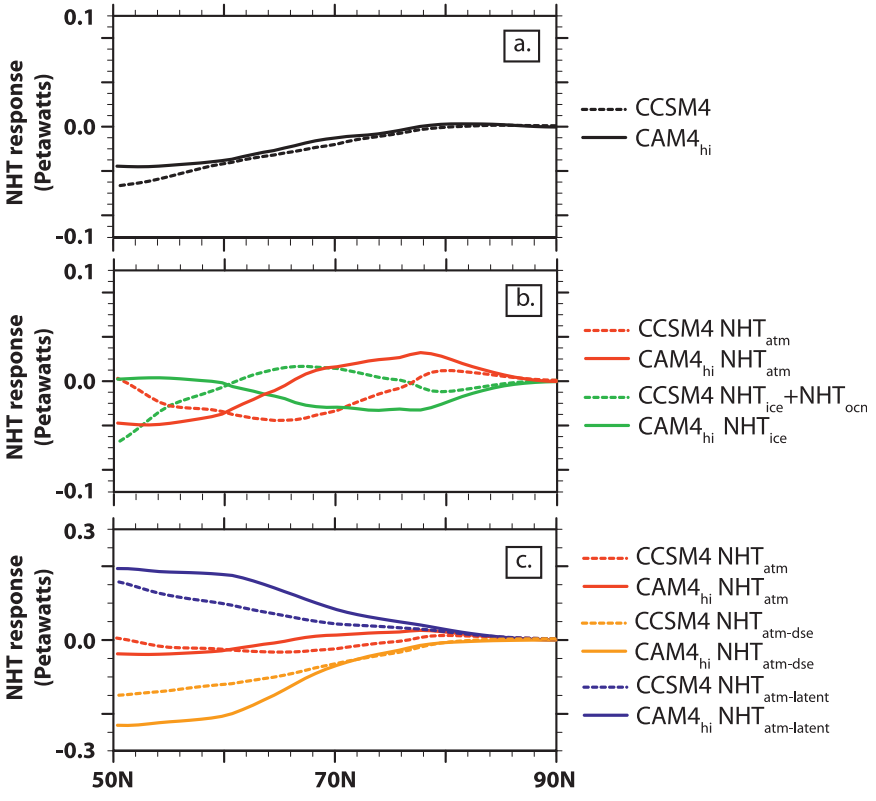

FIG. 8. Zonal mean equilibrium NHT response to 2 × CO_2 in coupled climate models with equivalent atmospheric components and resolution but differing ocean coupling (CCSM4 and $CAM4_{hi}$): (a) total NHT response, (b) NHT_{atm}, NHT_{ice}, and NHTocn response, and (d) NHT_{atm}, $NHT_{atm\text{-}latent}$, and $NHT_{atm\text{-}dse}$ response.

1) GLOBAL FEEDBACK ANALYSIS

Globally, an external forcing, such as the 2 × CO_2 radiative forcing Q_{2xCO2} imposed in our experiments, is balanced by a net radiative response at the TOA (ΔH, W m^{-2}) and changes in the net annual surface flux (ΔF, W m^{-2}). Setting $\Delta F = 0$, which is appropriate for our SOM experiments, and normalizing by the 2-m surface air temperature ($T_{s\text{-}air}$, K) response, a climate feedback parameter λ, with units of watts per square meter per Kelvin, can be defined. Following the notation of Gregory and Mitchell 1997, hereafter GM97), but changing their sign convention such that all fluxes are positive net downward and all feedbacks are positive when they enhance warming:

$$\lambda = \frac{\Delta H}{\Delta T_{s\text{-}air}} = \frac{\Delta N - Q_{2xCO2}}{\Delta T_{s\text{-}air}} = \frac{(\Delta N_{lw} + \Delta N_{sw}) - Q_{2xCO2}}{\Delta T_{s\text{-}air}}. \quad (2)$$

Assuming a linear response to the forcing, ΔH can be estimated in a transient simulation using Q_{2xCO2} and the change in the net downward TOA flux (ΔN, W m^{-2}) resulting from both the warming and the imposed radiative forcing. At equilibrium, $Q_{2xCO2} = -\Delta H$ and $\Delta N = 0$.

Analysis of λ is most useful when λ can be decomposed into feedback parameters associated with specific processes. Thus, we decomposed λ to identify the energetically dominant processes controlling the climate model response.

We partitioned λ into shortwave and longwave components and into clear-sky and cloud forcing components:

$$\lambda = \lambda_{lw} + \lambda_{sw} = \lambda_{lwclr} + \lambda_{lwcf} + \lambda_{swclr} + \lambda_{swcf}, \quad (3a)$$

$$\lambda_{lw} = \frac{\Delta N_{lw} - Q_{2xCO2}}{\Delta T_{s\text{-}air}}, \quad (3b)$$

$$\lambda_{sw} = \frac{\Delta N_{sw}}{\Delta T_{s\text{-}air}}, \quad (3c)$$

$$\lambda_{lwclr} = \frac{\Delta N_{lwclr} - Q_{2xCO2}}{\Delta T_{s\text{-}air}}, \quad (3d)$$

$$\lambda_{\text{lwcf}} = \frac{\Delta N_{\text{lw}} - \Delta N_{\text{lwclr}}}{\Delta T_{\text{s-air}}}, \tag{3e}$$

$$\lambda_{\text{swclr}} = \frac{\Delta N_{\text{swclr}}}{\Delta T_{\text{s-air}}}, \tag{3f}$$

and

$$\lambda_{\text{swcf}} = \frac{\Delta N_{\text{sw}} - \Delta N_{\text{swclr}}}{\Delta T_{\text{s-air}}}, \tag{3g}$$

where ΔN_{lw} and ΔN_{sw} are the change in the net (down minus up) shortwave and longwave TOA radiative fluxes at equilibrium, and ΔN_{lwclr} and ΔN_{swclr} are the changes in the net clear-sky TOA radiative fluxes at equilibrium.

We also used simplified radiative transfer to partition TOA shortwave radiative flux changes resulting from surface, cloud, and clear-sky processes using the approximate partial radiative perturbation (APRP) technique (Taylor et al. 2007). APRP enabled calculation of the following feedback parameters: shortwave surface ($\lambda_{\text{sw,aprp-surface}}$), shortwave cloud ($\lambda_{\text{sw,aprp-cld}}$), and shortwave clear sky ($\lambda_{\text{sw,aprp-clr}}$). Errors resulting from the simplified radiative transfer used in APRP produced differences between the estimated APRP shortwave feedbacks and λ_{sw}.

Table 2 contains global forcing, equilibrium warming, and feedback parameter analysis results. The global $Q_{2\text{xCO2}}$ is 9% larger in CAM5 than in CAM4, a difference that helps explain why CAM5 warms more than CAM4 (Table 1). That being said, the shortwave cloud forcing feedback difference between CAM4 and CAM5 is larger than any other global feedback difference. Consistent with more global warming in CAM5 than in CAM4, the global shortwave cloud feedbacks mitigated global warming in CAM4 ($\lambda_{\text{swcf}} = -0.15\ \text{W m}^{-2}\ \text{K}^{-1}$), but enhanced global warming in CAM5 ($\lambda_{\text{swcf}} = +0.39\ \text{W m}^{-2}\ \text{K}^{-1}$). Similar to the adjusted λ_{swcf} results in Gettelman et al. (2012), our APRP shortwave cloud feedback results indicate that global shortwave cloud feedbacks are positive in both CAM versions, but larger in CAM5 than in CAM4 (Fig. 9). In summary, both our results and Gettelman et al. (2012) indicate that positive shortwave cloud feedbacks are larger in CAM5 than in CAM4 and that shortwave cloud feedback differences help explain the greater global $2 \times CO_2$ warming in CAM5 than in CAM4.

TABLE 2. Global $2 \times CO_2$ forcing, temperature response and feedbacks. All feedbacks are positive when they enhance warming, unit $\text{W m}^{-2}\ \text{K}^{-1}$, are calculated after taking temporal and spatial averages, and are normalized by $\Delta T_{\text{s-air}}$.

	CAM4	CAM5
Forcing, $Q_{2\text{xCO2}}$ (W m^{-2})	3.5	3.8
Surface air temperature response, $\Delta T_{\text{s-air}}$ (K)	3.2	4.1
Total feedback, λ ($\text{Wm}^{-2}\ \text{K}^{-1}$)	−1.11	−1.00
Longwave feedback, λ_{lw}	−1.90	−2.04
Longwave clear feedback, λ_{lwclr}	−1.82	−1.78
Longwave cloud feedback, λ_{lwcf}	−0.09	−0.25
Shortwave feedback, λ_{sw}	0.80	1.04
Shortwave clear-sky feedback, λ_{swclr}	0.95	0.65
Shortwave cloud forcing feedback, λ_{swcf}	−0.15	0.39
Shortwave APRP surface feedback, $\lambda_{\text{sw,aprp-surface}}$	0.44	0.50
Shortwave APRP cloud feedback, $\lambda_{\text{sw,aprp-cld}}$	0.04	0.59
Shortwave APRP clear-sky feedback, $\lambda_{\text{sw,aprp-clr}}$	0.11	0.11

2) Extending global feedback analysis methods to the Arctic

Several issues emerge when implementing global feedback analysis methods described above in the Arctic. First, the Arctic surface air temperature warming ($\Delta T_{\text{s-air,A}}$) does not represent the heat content change of the Arctic system (e.g., B09). For example, feedback parameters using $\Delta T_{\text{s-air,A}}$ as a normalizing temperature overestimate feedback strength whenever there is latent heat consumed by sea ice melt. To address this concern, we examined Arctic feedback parameters normalized by an adjusted surface temperature change ($\Delta T_{\text{adj,A}}$). Over land areas we set $\Delta T_{\text{adj,A}}$ to $\Delta T_{\text{s,A}}$, while over the Arctic Ocean we set $\Delta T_{\text{adj,A}}$ to the ocean mixed layer temperature change adjusted for the latent heat required to melt all available sea ice. Because CAM4 has more summer latent heat consumption due to sea ice melting than CAM5 in response to $2 \times CO_2$ (not shown), using $\Delta T_{\text{adj,A}}$ as a normalizing temperature decreased the assessed Arctic feedback differences between the two models. That said, the normalizing temperature used in the calculation of the feedback parameters did not change the qualitative conclusions about the processes controlling the surface warming and amplification response differences.

Second, advection must be incorporated to close the Arctic energy budget and calculate feedback parameters based on TOA fluxes. While methods to incorporate advection into feedback parameter analysis have been developed (e.g., Boer and Yu 2003), we implemented a simple extension of the global feedback analysis framework. We started with Eq. (2), replaced the global values with Arctic values, and defined a local feedback parameter for the Arctic, λ_{A}:

$$\lambda_{\text{A}} = \frac{\Delta H_A}{\Delta T_{\text{adj,A}}} = \frac{\Delta N_{\text{A}} - Q_{\text{2xCO2,A}}}{\Delta T_{\text{adj,A}}} = \frac{(\Delta N_{\text{lw,A}} + \Delta N_{\text{sw,A}} + \Delta \text{NHT}^{*}_{\text{A}} \text{SA}^{-1}_{\text{A}}) - Q_{\text{2xCO2,A}}}{\Delta T_{\text{adj,A}}}, \tag{4}$$

where ΔNHT_A is the total NHT change into the Arctic basin (W) and SA_A is the surface area of the Arctic (m^2).

Like its global equivalent, λ_A can be decomposed into individual feedbacks. As a result, we write the Arctic equation corresponding to Eq. (3) including a new feedback associated with northward heat transport $\lambda_{NHT,A}$:

$$\lambda_A = \lambda_{lw,A} + \lambda_{sw,A} + \lambda_{NHT,A}, \quad (5a)$$

$$\lambda_{lw,A} = \frac{\Delta N_{lw,A} - Q_{2xCO2,A}}{\Delta T_{adj,A}}, \quad (5b)$$

$$\lambda_{sw,A} = \frac{\Delta N_{sw,A}}{\Delta T_{adj,A}}, \quad \text{and} \quad (5c)$$

and

$$\lambda_{NHT,A} = \frac{\Delta NHT_A^* SA_A^{-1}}{\Delta T_{adj,A}}, \quad (5d)$$

Heat transport feedbacks such as $\lambda_{NHT,A}$ can be calculated for any region. The global heat transport feedback is zero.

Finally, common feedback parameter techniques used for global feedback analysis are not always appropriate in the Arctic. For example, we did not separate $\lambda_{sw,A}$ into cloud and clear-sky shortwave feedbacks using Eqs. (3f–g). In both CAM4 and CAM5, the Arctic clear-sky shortwave flux 2 × CO_2 response was larger than the Arctic all-sky shortwave flux 2 × CO_2 response. In addition, large corrections were required to adjust Arctic cloud feedbacks for noncloud effects using the methods described in Shell et al. 2008, casting some doubt as to their validity. As a result, the use of the APRP was especially important for diagnosing the underlying causes for differing Arctic shortwave feedbacks in CAM4 and CAM5.

Table 3 contains the Arctic forcing, equilibrium warming, and feedback analysis results. Because the Arctic has a relatively small lapse rate, $Q_{2xCO2,A}$ is smaller than its global equivalent Q_{2xCO2} (W06). In both CAM4 and CAM5 the Arctic forcing was approximately three quarters of the global forcing (~74%). Taking this forcing difference alone, the Arctic would warm less than the global mean. Yet, as in all climate models, Arctic amplification occurs in our 2 × CO_2 experiments (Fig. 1–5), indicating strong positive Arctic feedbacks are present. In addition, because both CAM4 and CAM5 have a similar ratio of global to Arctic 2 × CO_2 forcing, feedback differences must explain their surface temperature amplification differences (Fig. 1c).

TABLE 3. As in Table 2 but for Arctic 2 × CO_2 forcing.

	CAM4	CAM5
Forcing, $Q_{2xCO2,A}$ (W m^{-2})	2.6	2.8
Surface air temperature response, $\Delta T_{s\text{-}air,A}$ (K)	7.0	10.0
Adjusted temperature response, $\Delta T_{adj,A}$ (K)	6.1	7.3
Total feedback, λ_A (W m^{-2} K^{-1})	−0.42	−0.38
Northward heat transport feedback, $\lambda_{NHT,A}$	0.07	−0.18
Longwave feedback, $\lambda_{lw,A}$	−1.43	−1.89
Longwave clear feedback, $\lambda_{lwclr,A}$	−2.07	−2.39
Longwave cloud feedback, $\lambda_{lwcf,A}$	0.64	0.49
Shortwave feedback, $\lambda_{sw,A}$	0.95	1.70
Shortwave APRP surface feedback, $\lambda_{sw,aprp\text{-}surface}$	1.68	3.07
Shortwave APRP cloud feedback, $\lambda_{sw,aprp\text{-}cld}$	−1.98	−0.32
Shortwave APRP clear-sky feedback, $\lambda_{sw,aprp\text{-}clr}$	0.14	0.19

Comparing global and Arctic feedback parameters allows us to identify which processes are important for Arctic surface amplification in CAM4 and CAM5 (Table 2, Table 3, Fig. 9). In both models the Arctic heat transport feedback $\lambda_{NHT,A}$ is relatively small when compared to the radiative feedbacks $\lambda_{lw,A}$ and $\lambda_{sw,A}$. In addition, the Arctic heat transport feedback $\lambda_{NHT,A}$ is negative in CAM5, the model that has the most surface warming. Both of these findings suggesting heat flux convergence into the Arctic does not explain surface amplification. Based on the feedback parameters, both longwave and shortwave radiative feedbacks affect surface amplification: shortwave clear-sky feedbacks and longwave cloud feedbacks enhance surface amplification, while shortwave cloud feedbacks and longwave clear-sky feedbacks oppose surface amplification. Consistent with the loss of Arctic snow and sea ice, the surface albedo feedback parameter $\lambda_{sw,aprp\text{-}surface}$ is more positive than its global equivalent in both models and explains why shortwave surface feedbacks enhance surface amplification.

We next use the feedback parameters to explain why CAM5 has more Arctic surface warming and amplification than CAM4 (Table 3, Fig. 9). Consistent with Figs. 6 and 7, northward heat transport feedback ($\lambda_{NHT,A}$) differences do not explain Arctic warming differences: CAM4 has a small positive $\lambda_{NHT,A}$ while CAM5 has a small negative $\lambda_{NHT,A}$. Instead, local feedback strength differences explain why CAM5 warms even more than CAM4. While both models have strong positive Arctic shortwave feedbacks, they are stronger in CAM5 ($\lambda_{sw,A}$ = 1.70 W m^{-2} K^{-1}) than in CAM4 ($\lambda_{sw,A}$ = 0.95 W m^{-2} K^{-1}). The Arctic APRP results show that both the positive shortwave surface feedback $\lambda_{sw,aprp\text{-}surface}$ and the negative shortwave cloud feedback $\lambda_{sw,aprp\text{-}cld}$, lead to greater Arctic warming in CAM5 than in CAM4. Longwave feedback differences are present, but they do not explain Arctic warming differences in CAM4 and CAM5. Longwave clear-sky

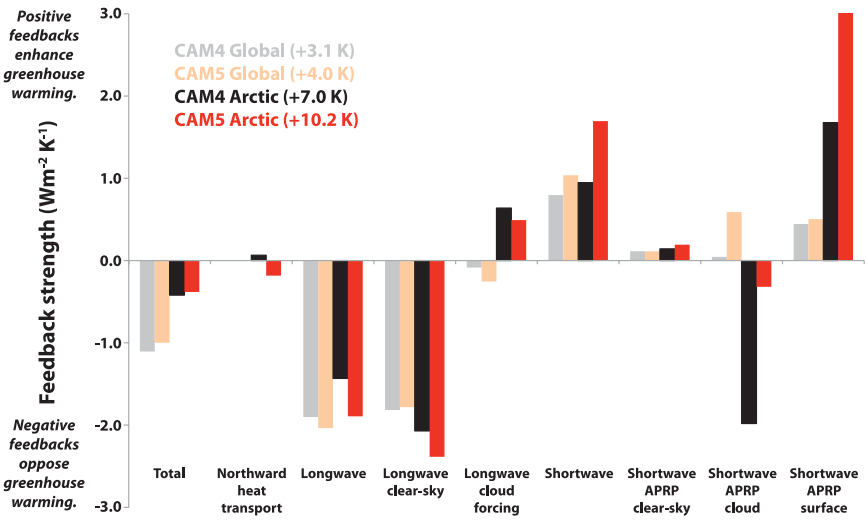

FIG. 9. Global and Arctic feedback parameters in CAM4 and CAM5. The equilibrium surface air temperature warming is indicated after the model name and geographic region. See also Tables 2 and 3.

feedbacks are more negative in CAM5 than in CAM4, and CAM5 has a smaller positive longwave cloud feedback than CAM4.

c. Are there properties of the mean state that are consistent with the largest feedback differences between CAM4 and CAM5?

Using feedback analysis, we found that local shortwave feedback differences explain the larger equilibrium Arctic climate response to increased greenhouse gases in CAM5 as compared to CAM4 (Fig. 9, Table 3). Numerous physical parameterization differences produce these local shortwave feedback differences, and evidence of these parameterization differences may be present in the 1850 climate state. As such, we next describe aspects of the 1850 control climates in CAM4 and CAM5 that are consistent with their feedback differences.

We first examine the monthly evolution of Arctic net energy flux at the surface and the TOA (Fig. 10). While the seasonality of net energy flux is similar in the 1850 control of both models, the seasonal range at the surface (min–max) is 40 W m^{-2} greater in CAM5 than in CAM4: 134 W m^{-2} versus 94 W m^{-2}. Similarly, CAM5 has a larger seasonal energy flux range than CAM4 by 36 W m^{-2} at the TOA. The energy flux differences between CAM4 and CAM5 are more evident in summer than in other seasons. When compared to CAM4, CAM5 has a larger vertical pulse of heat in and out of the Arctic in response to seasonal solar forcing.

In a warmer Arctic world, the range of net flux values increases, becoming both more positive in summer and more negative in winter (Fig. 10c). Interestingly, this enhancement is larger in CAM5 than in CAM4 (Fig. 10c), a response difference that matches their control climate flux differences (Fig. 10a,b).

Comparing cloud fractions (Fig. 11a) and energy fluxes (Figs. 10a,b) shows that cloud fraction differences cannot explain these identified energy flux differences. CAM4 and CAM5 have similar summer cloud fractions, but have 30 W m^{-2} differences in their July net surface energy flux. Assuming identical cloud optical properties, the reduced winter cloud fractions in CAM4 should allow more longwave radiation escape to space and result in a more negative net energy flux in CAM4 than in CAM5. Yet, the winter net energy flux is more negative in CAM5 than in CAM4 (Figs. 10a,b), and CAM5 is colder during winter than CAM4 (Fig. 2a).

In contrast to cloud fraction differences, cloud property differences in the 1850 control climates of CAM4 and CAM5 do explain their energy flux differences. Throughout the annual cycle, the Arctic clouds in CAM4 have significantly larger liquid cloud water paths (Fig. 11b) and visible cloud optical depths (not shown) than the Arctic clouds in CAM5. For example, during summer (JJA), the visible optical depth of Arctic clouds in CAM4 (23.3) is more than 5 times that in CAM5 (4.4). These cloud water path (CWP) and cloud optical property differences are consistent with CAM5 having a more positive summer net energy fluxes and a more negative winter net energy fluxes than CAM4 (Figs. 10a,b). During midsummer, when shortwave radiation dominates Arctic energy fluxes, optically thin

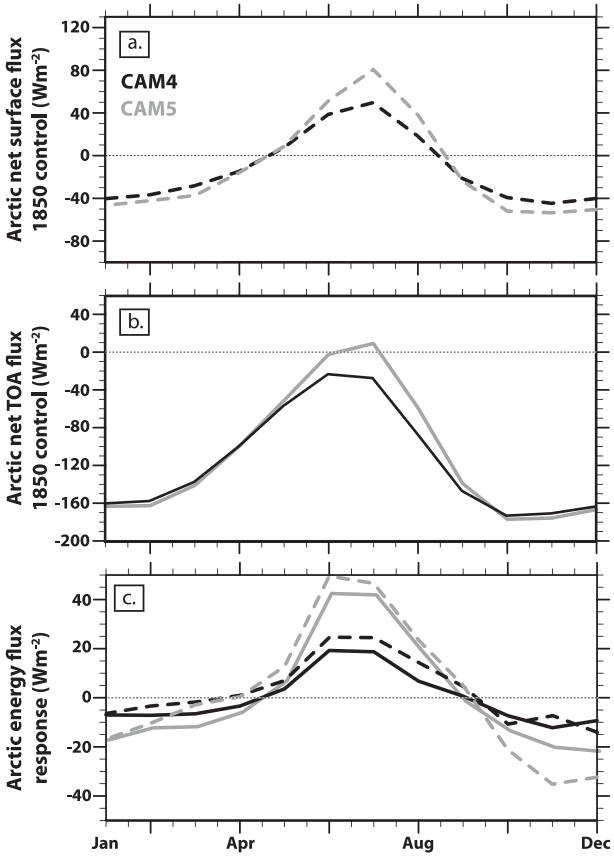

FIG. 10. Monthly evolution of Arctic energy fluxes in CAM4 and CAM5: (a) surface net energy fluxes in 1850 controls, (b) TOA net energy fluxes in 1850 controls, and (c) surface (dashed) and TOA (solid) net energy flux response to 2 × CO_2.

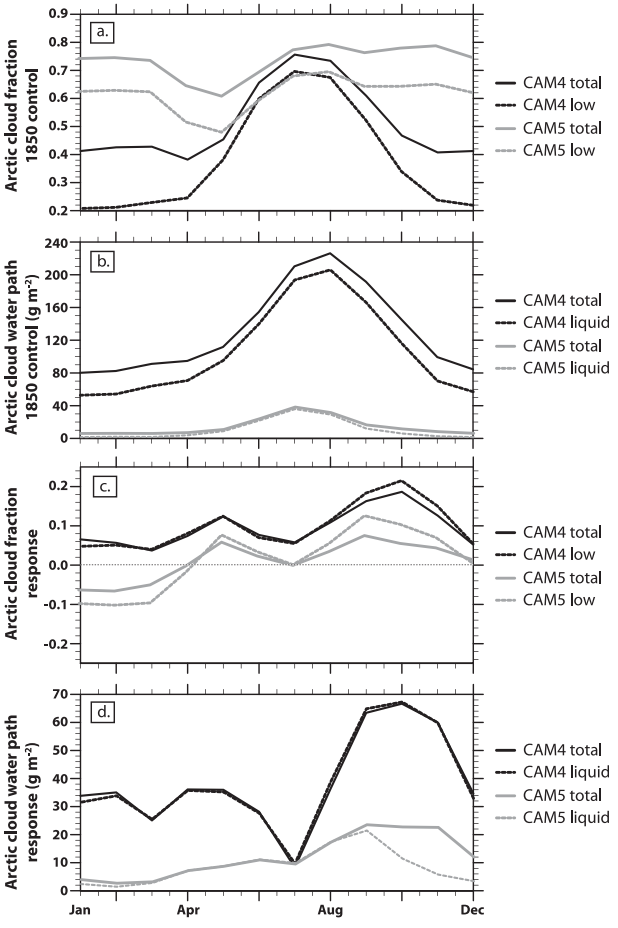

FIG. 11. Monthly evolution of Arctic clouds in CAM4 and CAM5: (a) total and low cloud fraction, b) gridbox total and liquid cloud water path, (c) total and low cloud fraction, and (d) gridbox total and liquid cloud water path response.

clouds in CAM5 allow more shortwave radiation to reach the surface and be absorbed. This increased absorbed shortwave radiation increases the net positive shortwave radiation and thus, the positive net summer flux. During winter, when longwave radiation dominates Arctic energy budgets, optically thin clouds in CAM5 allow more longwave radiation to escape to space. This increased outgoing longwave radiation decreases both the negative net longwave radiation and the negative net winter flux.

The cloud fraction, cloud water path, and cloud optical depth responses are all consistent with more negative shortwave cloud feedbacks and more positive longwave cloud feedbacks in CAM4 as compared to CAM5 (Fig. 9, Table 3). The modeled Arctic cloud response to 2 × CO_2 forcing is dominated by low liquid cloud response (Figs. 11c,d). CAM4 Arctic cloud cover increases in all months (Fig. 10c) and over all surfaces (not shown). In contrast, the sign of the CAM5 cloud response varies with season (Fig. 10c) and surface type (not shown). In both CAM4 and CAM5, liquid cloud water path increases in response to 2 × CO_2 (Fig. 10d), but is consistent with their 1850 control climate differences (Fig. 10b), CAM4 has larger liquid cloud water path increases than CAM5 in every month except July. When annually averaged, the liquid cloud water path increases are 4.6 larger in CAM4 than in CAM5. During summer [June–August (JJA)], the liquid cloud water path differences lead a larger increase in in-cloud liquid visible optical depth in CAM4 (+4.2) than in CAM5 (+1.5). When compared to CAM5, the larger increases in cloud fraction, cloud water path, and cloud optical depth in CAM4 are all consistent with smaller changes in the seasonal range in net energy fluxes (Figs. 10c).

In addition to clouds, surface conditions influence Arctic energy fluxes and the Arctic response to external forcing. Thus, we compare the geographic distribution of and variability in Arctic sea ice extent and thickness in

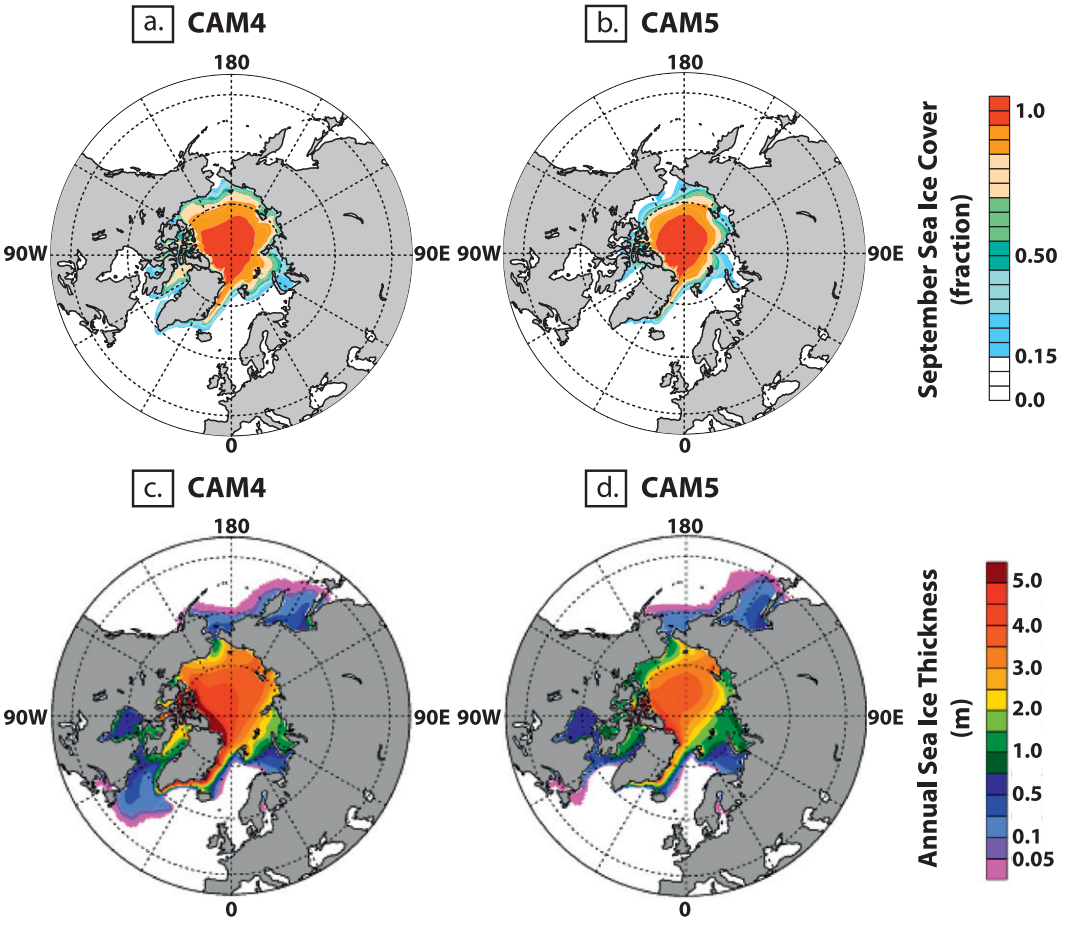

FIG. 12. Arctic sea ice in the CAM4 and CAM5 1850 control integrations: (a) CAM4 September ice fraction, (b) CAM5 September ice fraction, (c) CAM4 annual mean sea ice thickness, and (d) CAM5 annual mean ice thickness.

the 1850 control integrations. CAM5 has less extensive (Fig. 12a, Fig. 2b) and thinner (Fig. 12b) ice than CAM4. Like the clouds, the sea ice differences between CAM4 and CAM5 help explain Arctic energy flux differences. As expected from Bitz (2008), HB03, and Rind et al. (1995), relatively thin ice may also be enhancing the Arctic climate response in CAM5 as compared to CAM4.

4. Discussion

This study explains the equilibrium Arctic response to increased greenhouse gases in climate models with different atmospheric components (CAM4, CAM5) and different degrees of ocean coupling (mixed layer ocean, full-depth ocean). The main strengths of this study are that it evaluates all factors thought to be important to the modeled Arctic $2 \times CO_2$ climate response and that it isolates the influence of atmospheric physics and ocean model complexity. The most significant finding is that local feedbacks, not heat transport into the Arctic basin, are the dominant control on the equilibrium Arctic surface climate response.

The largest Arctic surface warming and amplification occurs in CAM5, a model with relatively large radiative forcing for $2 \times CO_2$, relatively weak negative Arctic shortwave cloud feedbacks, and relatively strong positive Arctic shortwave surface albedo feedbacks. That the strength of Arctic surface albedo feedbacks and Arctic shortwave cloud feedbacks are anticorrelated in CAM5 and CAM4 is consistent with their Arctic low liquid cloud differences. When optically thick clouds block incoming shortwave radiation, they obscure underlying surface albedo changes and reduce the efficacy of surface albedo feedbacks. That non-SAF feedbacks are important for explaining model differences is consistent with W06, who used feedback parameter analysis to show that non-SAF shortwave feedbacks that oppose Arctic surface temperature amplification explain intermodel spread in Arctic surface temperature amplification, and also with Donohoe

and Battisti 2011 who found that intermodel spread in shortwave radiation reflected by the atmosphere is three times larger than intermodel spread in shortwave radiation reflected by the surface.

In our experiments, models with more global warming also have more Arctic warming. Given this result, it is intriguing that northward heat transport differences do not explain the largest Arctic climate response differences that we found. Changes in atmospheric heat transport into the Arctic were of the opposite sign to explain large Arctic surface warming response differences in CAM4 and CAM5, a result consistent with Hwang et al. 2011. Although ocean heat transport increases do slightly enhance sea ice loss in CCSM4, simple extrapolations show that the equilibrium Arctic $2 \times CO_2$ response in CCSM4 is very unlikely to be as large as it is in CAM5. Interestingly, we found similar total $2 \times CO_2$ heat transport changes at high northern latitudes may help explain a similar $2 \times CO_2$ climate response in models with different ocean model complexity (CCSM4 versus $CAM4_{hi}$ in Fig. 1, Fig. 8). That ocean heat transport plays a minor role in explaining the differing model responses in this study may seem at odds with previous studies (e.g., HB03; R07; Mahlstein and Knutti 2011; Rose and Ferreira 2012). One potential explanation is that the ocean is more important to the transient response than it is to the equilibrium response, a topic not addressed here.

Owing to the idealistic nature of the model experiments used in this study, assessing the accuracy of their equilibrium response to increased greenhouse forcing is not easy. Present-day simulations using CAM4 and CAM5 (not shown) bracket observations of TOA energy fluxes from Clouds and the Earth's Radiant Energy System (CERES) (Loeb et al. 2009). Consistent with present-day observations (e.g., Kay and Gettelman 2009), Arctic clouds in both CAM versions are dominated by low clouds. de Boer et al. (2012) show that CAM4 underestimates present-day winter Arctic cloud fractions when compared to satellite- and ground-based cloud observations. Instrument simulators, which enable robust comparisons to observations by using consistent definition of cloud, show that CAM5 cloud fractions are more realistic than CAM4 cloud fractions both globally and in the Arctic (Kay et al. 2012). Comparisons using present-day model configurations show that CAM4 has excessive Arctic liquid CWP when compared to ground-based observations (Shupe et al. 2005), while CAM5 is at the opposite extreme (not shown). While an in-depth evaluation of CAM4 and CAM5 with observations is beyond the scope of this work, the results here motivate additional evaluation with observations and targeted diagnostics.

Finally, this study documents the processes controlling the equilibrium Arctic response to a CO_2 doubling in CESM coupled model variants. As such, the processes that explain the Arctic greenhouse responses here are not necessarily universal, especially for explaining intermodel spread in transient climate projections. For example, although we find suggestive and physically consistent relationships between the control climate energy fluxes in CAM4 and CAM5 and their equilibrium $2 \times CO_2$ Arctic response, we find little relationship between the control climate energy fluxes and transient Arctic warming in CMIP3 models (not shown).

5. Summary

This study investigates the processes controlling the equilibrium Arctic climate response to an instantaneous CO_2 doubling in recent state-of-the-art coupled climate model experiments using CESM. The main findings are as follows.

1) The representation of atmospheric processes (CAM4 versus CAM5) has a larger influence on the equilibrium Arctic response to $2 \times CO_2$ than the complexity of the ocean model (slab ocean versus full-depth ocean) (Table 1, Fig. 1, Fig. 2). Though ocean northward heat transport into the Arctic increases when a full-depth ocean model is used, the impact of ocean model complexity on the equilibrium Arctic climate response to $2 \times CO_2$ is modest.
2) Radiative forcing and feedbacks are more important than northward heat transport for explaining the amplified equilibrium Arctic surface climate response to increased greenhouse gases (Fig. 9, Tables 2 and 3). The model with the greatest equilibrium Arctic warming (CAM5) has more $2 \times CO_2$ radiative forcing, more positive Arctic shortwave surface albedo feedbacks, and less negative Arctic shortwave cloud feedbacks (Fig. 9, Table 3). The influence of low-level liquid Arctic clouds on Arctic shortwave cloud and surface albedo feedbacks is especially important for explaining Arctic response differences found in this study (Fig. 9, Fig. 11).
3) The vertical structure of Arctic warming and longwave radiative feedbacks respond to the surface warming magnitude, but do not explain the intermodel equilibrium $2 \times CO_2$ surface warming differences found in this study (Figs. 3–4, Fig. 9).

While the described differences in equilibrium Arctic climate response to increased greenhouse gases are alarming, this study shows that climate model experiments that can isolate the influence of model physics and model complexity provide a useful laboratory for

identifying and understanding the processes controlling Arctic climate response to external forcing.

Acknowledgments. JEK thanks Brian Medeiros, Karen Shell, Karl Taylor, Jack Chen, and Ben Sanderson for scientific discussions that improved this manuscript, Gokhan Danabasoglu for running the CCSM4 simulations, and Cecile Hannay for running the CAM5 simulations. This work was funded by the United States National Science Foundation (NSF) through NCAR, NSF Grant ARC-0909313 and by NASA Grant 08-MAP-117. The authors also acknowledge high-performance computing support provided by NCAR's Computational and Information Systems Laboratory, sponsored by NSF.

APPENDIX

Northward Heat Transport Calculation Methods

Assuming no atmospheric heat storage ($\partial E_{\text{atm}}/\partial t = 0$), which is appropriate for equilibrium conditions, vertically integrated total northward heat transport (NHT) and atmospheric northward heat transport (NHT_{atm}) can be deduced from diabatic heating (e.g., Porter et al. 2010). As such, NHT and NHT_{atm} across each latitude band shown in Fig. 6 and Fig. 8 were calculated using top of atmosphere and surface energy fluxes as follows:

$$\text{NHT} = -2\pi R_e^2 \int_{\varphi}^{\pi/2} N \cos(\varphi)\, d\varphi \qquad \text{(A1)}$$

and

$$\text{NHT}_{\text{atm}} = -2\pi R_e^2 \int_{\varphi}^{\pi/2} (N - n) \cos(\varphi)\, d\varphi, \qquad \text{(A2)}$$

where R_e is radius of the earth (m), N is the net TOA energy flux (W m^{-2}, positive when the combined atmosphere and surface energy increases), and n is the net surface energy flux (W m^{-2}, positive when surface energy increases).

Fluxes N and n were calculated from 10-yr averages of CAM outputs using

$$N = N_{\text{sw}} + N_{\text{lw}}, \qquad \text{(A3)}$$

where N_{lw} and N_{sw} are net (down minus up) shortwave and longwave TOA radiation, both in watts per square meter:

$$n = n_{\text{sw}} + n_{\text{lw}} + n_{\text{sh}} + n_{\text{lh}}, \qquad \text{(A4)}$$

where n_{lw} and n_{sw} are net (down minus up) shortwave and longwave surface radiative fluxes, and n_{sh} and n_{lh} (down minus up) are the net surface sensible and latent heat fluxes, all in watts per square meter.

Because the default CAM n_{lh} output (LHFLX) does not account for latent heat consumed during snowmelt, n_{lh} was calculated using

$$n_{\text{lh}} = -(L_f \rho_w \text{PREC}_{\text{snow}}) - \text{LHFLX}, \qquad \text{(A5)}$$

where L_f is the latent heat of fusion (J kg^{-1}), $\text{PREC}_{\text{snow}}$ is the water equivalent snow precipitation rate (m s^{-1}), and ρ_w is the density of water (kg m^{-3}).

To build confidence in the NHT_{atm} estimates based on Eqs. (A2)–(A5), the nonatmospheric vertically integrated NHT ($\text{NHT}_{\text{non-atm}}$) derived from residual methods was compared to the sum of inline calculations of the vertically integrated ice and ocean northward heat transport, NHT_{ocn} and NHT_{ice}. The two should be equal:

$$\text{NHT}_{\text{non-atm}} = \text{NHT} - \text{NHT}_{\text{atm}} = \text{NHT}_{\text{ocn}} + \text{NHT}_{\text{ice}}. \qquad \text{(A6)}$$

The differences resulting from the two methods of estimating $\text{NHT}_{\text{non-atm}}$ were small, less than 0.002 PW (~2%), a difference that is not distinguishable in Fig. 6 or Fig. 8.

The latent atmospheric heat transport $\text{NHT}_{\text{atm-latent}}$ across each latitude band shown in Fig. 6 and Fig. 8 was calculated using

$$\text{NHT}_{\text{atm-latent}} = 2\pi R_e^2 \int_{\varphi}^{\pi/2} (LH_{\text{prec}} + n_{\text{lh}}) \cos\varphi\, d\varphi, \qquad \text{(A7)}$$

where LH_{prec} is the total latent heating in the atmosphere (W m^{-2}) calculated as

$$\text{LH}_{\text{prec}} = (L_v \rho_w (\text{PREC}_{\text{liq}} + \text{PREC}_{\text{snow}}) + L_f \rho_i \text{PREC}_{\text{snow}}), \qquad \text{(A8)}$$

where PREC_{liq} is the water equivalent rain precipitation rate (m s^{-1}), and ρ_i is the density of ice (kg m^{-3}).

The dry static energy atmospheric heat transport $\text{NHT}_{\text{atm-dse}}$ was then calculated as a residual using Eqs. (A2) and (A7):

$$\text{NHT}_{\text{atm-dse}} = \text{NHT}_{\text{atm}} - \text{NHT}_{\text{atm-latent}}. \qquad \text{(A9)}$$

The transient vertically integrated NHT_{atm} at 70°N shown in Fig. 7 was based on Arctic averaged (70°–90°N) monthly averaged CAM outputs using

$$\mathrm{NHT}_{\mathrm{atm}} = \left(\frac{\partial E_{\mathrm{atm}}}{\partial t} - N + n\right)\mathrm{SA}_{\mathrm{Arctic}}, \quad \text{(A10)}$$

where $\mathrm{SA}_{\mathrm{Arctic}}$ is the surface area of the Arctic (m^2), $\partial E_{\mathrm{atm}}/\partial t$ is the partial derivative atmospheric energy storage ($\mathrm{W\ m^{-2}}$) with atmospheric energy (E_{atm}) defined as:

$$E_{\mathrm{atm}} = \frac{1}{g}\int_0^{ps} (c_p T + k + L_v q + \Phi_s)\, dp, \quad \text{(A11)}$$

where p is pressure (Pa), p_s is the reference surface pressure (1000 hPa), g is gravitational acceleration ($\mathrm{m\ s^{-2}}$), c_p is the specific heat of dry air at constant pressure ($\mathrm{J\ K^{-1}\ kg^{-1}}$), T is the temperature (K), k is the kinetic energy ($\mathrm{J\ kg^{-1}}$), L_v is the latent heat of vaporization ($\mathrm{J\ kg^{-1}}$), q is the specific humidity ($\mathrm{kg\ kg^{-1}}$), and ϕ_s is the surface geopotential ($\mathrm{m^2\ s^{-2}}$).

REFERENCES

Alexeev, V. A., P. L. Langen, and J. R. Bates, 2005: Polar amplification of surface warming on an aquaplanet in ghost forcing experiments without sea ice feedbacks. *Climate Dyn.,* **24** (7–8), 655–666, doi:10.1007/s00382-005-0018-3.

Bitz, C. M., 2008: Some aspects of uncertainty in predicting sea ice thinning. *Arctic Sea Ice Decline: Observations, Projections, Mechanisms, and Implications, Geophys. Monogr.,* Vol. 180, Amer. Geophys. Union, 63–76.

——, P. R. Gent, R. A. Woodgate, M. M. Holland, and R. Lindsay, 2006: The influence of sea ice on ocean heat uptake in response to increasing CO_2. *J. Climate,* **19,** 2437–2450.

——, J. K. Ridley, M. M. Holland, and H. Cattle, 2012a: 20th and 21st century Arctic climate in global climate models. *Arctic Climate Change—The ACSYS Decade and Beyond,* P. Lemke, Ed., Springer, 405–436.

——, K. M. Shell, P. R. Gent, D. Bailey, G. Danabasoglu, K. C. Armour, M. M. Holland, and J. T. Kiehl, 2012b: Climate sensitivity of the Community Climate System Model, version 4. *J. Climate,* **25,** 3053–3070.

Boé, J., A. Hall, and X. Qu, 2009: Current GCMs' unrealistic negative feedback in the Arctic. *J. Climate,* **22,** 4682–4695.

Boer, G. J., and B. Yu, 2003: Climate sensitivity and response. *Climate Dyn.,* **20,** 415–429.

de Boer, G., and Coauthors, 2012: A characterization of the present-day Arctic atmosphere in CCSM4. *J. Climate,* **25,** 2676–2695.

Donohoe, A., and D. S. Battisti, 2011: Atmospheric and surface contributions to planetary albedo and their relationship to the total meridional energy transport. *J. Climate,* **24,** 4401–4417.

Gent, P. R., and Coauthors, 2011: The Community Climate System Model, version 4. *J. Climate,* **24,** 4973–4991.

Gettelman, A., J. E. Kay, and K. Shell, 2012: The evolution of climate sensitivity and climate feedbacks in the Community Earth System Model. *J. Climate,* **25,** 1453–1469.

Gorodetskaya, I. V., L. B. Tremblay, B. Liepert, M. A. Cane, and R. I. Cullather, 2008: The influence of cloud and surface properties on the Arctic Ocean shortwave radiation budget in coupled models. *J. Climate,* **21,** 866–882.

Graversen, R. G., and M. Wang, 2009: Polar amplification in a coupled climate model with locked albedo. *Climate Dyn.,* **33,** 629–643.

Gregory, J. M., and J. F. B. Mitchell, 1997: The climate response to CO_2 of the Hadley Centre coupled AOGCM with and without flux adjustment. *Geophys. Res. Lett.,* **24,** 1943–1946.

——, P. A. Stott, D. J. Cresswell, N. A. Rayner, C. Gordon, and D. M. H. Sexton, 2002: Recent and future changes in Arctic sea ice simulated by the HadCM3 AOGCM. *Geophys. Res. Lett.,* **29,** 2175, doi:10.1029/2001GL014575.

——, and Coauthors, 2004: A new method for diagnosing radiative forcing and climate sensitivity. *Geophys. Res. Lett.,* **31,** L03205, doi:10.1029/2003GL018747.

Hall, A., 2004: Role of surface albedo feedback in climate. *J. Climate,* **17,** 1550–1568.

Hansen, J., and Coauthors, 2005: Efficacy of climate forcings. *J. Geophys. Res.,* **110,** D18104, doi:10.1029/2005JD005776.

Holland, M. M., and C. M. Bitz, 2003: Polar amplification of climate change in coupled models. *Climate Dyn.,* **21,** 221–232.

Hwang, Y.-T., D. W. Frierson, and J. E. Kay, 2011: Coupling between Arctic feedbacks and changes in poleward energy transport. *Geophys. Res. Lett.,* **38,** L17704, doi:10.1029/2011GL048546.

Kay, J. E., and A. Gettelman, 2009: Cloud influence on and response to seasonal Arctic sea ice loss. *J. Geophys. Res.,* **114,** D18204, doi:10.1029/2009JD011773.

——, and Coauthors, 2012: Exposing global cloud biases in the Community Atmosphere Model (CAM) using satellite observations and their corresponding instrument simulators. *J. Climate,* **25,** 5190–5207.

Kiehl, J. T., C. A. Shields, J. J. Hack, and W. D. Collins, 2006: The climate sensitivity of the Community Climate System Model version 3 (CCSM3). *J. Climate,* **19,** 2584–2596.

Langen, P. L., and V. A. Alexeev, 2007: Polar amplification as a preferred response in an aquaplanet GCM. *Climate Dyn.,* **29,** 305–317, doi:10.1007/s00382-006-0221-x.

Loeb, N. G., B. A. Wielicki, D. R. Doelling, G. L. Smith, D. F. Keyes, S. Kato, N. Manalo-Smith, and T. Wong, 2009: Toward optimal closure of the earth's top-of-atmosphere radiation budget. *J. Climate,* **22,** 748–766.

Mahlstein, I., and R. Knutti, 2011: Ocean heat transport as a cause for model uncertainty in projected Arctic warming. *J. Climate,* **24,** 1451–1460.

Manabe, S., and R. J. Stouffer, 1980: Sensitivity of a Global climate model to an increase of CO_2 concentration in the atmosphere. *J. Geophys. Res.,* **85** (C10), 5529–5554.

Medeiros, B., C. Deser, R. A. Tomas, and J. E. Kay, 2011: Arctic inversion strength in climate models. *J. Climate,* **24,** 4733–4740.

Miller, G. H., and Coauthors, 2010: Arctic amplification: Can the past constrain the future? *Quat. Sci. Rev.,* **29,** 1674–1790, 10.1016/j.quascirev.2010.02.008.

Neale, R. B., and Coauthors, 2011a: Description of the NCAR Community Atmosphere Model (CAM5). NCAR Tech. Rep. NCAR/TN-486+STR, 268 pp.

——, and Coauthors, 2011b: Description of the NCAR Community Atmosphere Model (CAM4). NCAR Tech. Rep. NCAR/TN-485+STR, 212 pp.

Porter, D. F., J. J. Cassano, M. C. Serreze, and D. N. Kindig, 2010: New estimates of the large-scale Arctic atmospheric energy budget. *J. Geophys. Res.,* **115,** D08108, doi:10.1029/2009JD012653.

Reichler, T., M. Dameris, and R. Sausen, 2003: Determination of tropopause height from gridded data. *Geophys. Res. Lett.,* **30,** 2042, doi:10.1029/2003GL018240.

Ridley, J., J. Lowe, C. Brierley, and G. Harris, 2007: Uncertainty in the sensitivity of Arctic sea ice to global warming in a perturbed parameter climate model ensemble. *Geophys. Res. Lett.,* **34,** L19704, doi:10.1029/2007GL031209.

Rind, D., and Coauthors, 1995: The role of sea ice in $2{\cdot}CO_2$ climate model sensitivity. Part I: The total influence of sea ice thickness and extent. *J. Climate,* **8,** 449–463.

Rose, B. E. J., and D. Ferreira, 2012: Ocean heat transport and water vapor greenhouse in a warm equable climate: A new look at the low gradient paradox. *J. Climate,* in press.

Serreze, M. C., and R. G. Barry, 2011: Processes and impacts of Arctic amplification: A research synthesis. *Global Planet. Change,* **77,** 85–96, doi:10.1016/j.gloplacha.2011.03.004.

——, and Coauthors, 2007: The large-scale energy budget of the Arctic. *J. Geophys. Res.,* **112,** D11122, doi:10.1029/2006JD008230.

——, and Coauthors, 2009: The emergence of surface-based Arctic amplification. *The Cryosphere,* **3,** 11–19.

Shell, K. M., J. T. Kiehl, and C. A. Shields, 2008: Using the radiative kernel technique to calculate climate feedbacks in NCAR's Community Atmosphere Model. *J. Climate,* **21,** 2269–2282.

Shupe, M. D., T. Uttal, and S. Y. Matrosov, 2005: Arctic cloud microphysics retrievals from surface-based remote sensors at SHEBA. *J. Appl. Meteor.,* **44,** 1544–1562.

Soden, B. J., and I. M. Held, 2006: An assessment of climate feedbacks in coupled atmosphere–ocean models. *J. Climate,* **19,** 3354–3360.

Solomon, S., D. Qin, M. Manning, M. Marquis, K. Averyt, M. M. B. Tignor, H. L. Miller Jr., and Z. Chen, Eds., 2007: *Climate Change 2007: The Physical Science Basis*. Cambridge University Press, 996 pp.

——, G. K. Plattner, R. Knutti, and P. Friedlingstein, 2009: Irreversible climate change due to carbon dioxide emissions. *Proc. Natl. Acad. Sci. USA,* **106,** 1704–1709.

Taylor, K. E., and Coauthors, 2007: Estimating shortwave radiative forcing and response in climate models. *J. Climate,* **20,** 2530–2543.

Winton, M., 2006: Amplified Arctic climate change: What does surface albedo feedback have to do with it? *Geophys. Res. Lett.,* **33,** L03701, doi:10.1029/2005GL025244.

——, K. Takahashi, and I. Held, 2010: Importance of ocean heat uptake efficacy to transient climate change. *J. Climate,* **23,** 2333–2344.